BJBMB

Biobacta Journal of Biochemistry and Molecular Biology

https://bjbmb.org

SPBH

Original article

Electrolytic Synthesis of Magnesium Oxide Nanoparticles (MgO NPs) for Dye-Sensitized Solar Cells Applications

Ghanem Abdulnabi Kazem

Ministry of Education / Karbala Education Directorate, Iraq

Email: murtada2002abd@gmail.com

DOI: https://doi.org/10.71428/BJBMB.2026.0202

Abstract

The present work reports a simple and comprehensive electrochemical approach for the production of magnesium oxide nanoparticles (MgO NPs) from magnesium chloride (MgCl2) solution under alkaline conditions and subsequent calcination at regulated temperatures. The mean crystalline particle size was determined by the Scherrer equation as 19.7+/-2.0 nm. Transmission electron microscopy (TEM) pictures revealed the formation of quasi-polyhedral particles of 20.3+/-3.8 nm with clear (200) lattice planes. SEM-EDX investigation revealed a consistent porosity structure with no visible defects.

The synthesized material was deposited over a titanium dioxide (TiO2) composite photoanode at a concentration of 5 wt%. The photoanode was then used for the fabrication of dye-sensitized solar cells (DSSCs). We have performed a detailed comparison of two forms of dye-sensitized pigments: the classical ruthenium compound N719 and the natural anthocyanin extract from fresh blackberries, i.e., the cyanidin-3-glucoside complex. In the photovoltaic experiments under AM 1.5G light, the power conversion efficiency (PCE) of the N719-sensitized cell was 4.8% while that of the cell using the natural dye was 2.1%. Observed performance differences are due to spectral absorption differences.

Keywords: MgO NPS, DSSCs, anthocyanins, X-ray diffraction, Scanning Electron Microscope

Introduction

1-1 General Context and Research Motivations

Securing the world's growing energy needs while reducing carbon emissions represents the most significant technological challenge of this century. Solar energy stands out as a promising strategic option capable of converting solar radiation into electrical energy in a scalable and sustainable manner, with a minimal environmental footprint. However, the prevailing technology based on crystalline silicon involves high production costs that limit its adoption in resource-limited contexts [1].

Dye-sensitized solar cells (DSSCs) have been considered as a technologically and economically feasible substitute for traditional p-n photovoltaic systems. The discipline emerged in the late 1960s when the generation of electricity in electrochemical cells using luminous organic dyes was identified. The first chlorophyll-sensitized zinc oxide (ZnO) electrode was reported by the University of California, Berkeley in 1972, demonstrating the conversion of light into energy through the passage of electrons from the excited dye molecules into a wide-bandgap semiconductor [2- 5].

A dye-sensitized solar cell is a device made up of a nanostructured layer of a semiconductor, usually

Received: April 15, 2026. Accepted: July 1, 2026. Published: August 8, 2026

titanium dioxide anatase (TiO2), on which a light-collecting dye is placed. A key problem with these cells is that the injected electrons recombine with the oxidized electrolyte at the semiconductor interface, lowering the open circuit voltage and overall efficiency. Magnesium oxide (MgO) has a large energy gap (~7.8 eV) and stable surface basicity, which can suppress back electron transport when MgO is included as a pass-through layer or a blocking layer to TiO2 photoanodes [6- 8].

We report here an easy and complete electrochemical route for the synthesis of magnesium oxide nanoparticles (MgO NPs) from magnesium chloride (MgCl2) solution in alkaline medium, followed by calcination at regulated temperatures. The mean crystalline particle size was 19.7±2.0 nm from the Scherrer equation. Transmission electron microscopy (TEM) pictures revealed quasi-polyhedral particles of 20.3±3.8 nm with clear (200) lattice planes. The SEM-EDX investigation showed a homogeneous porosity structure without any detectable defects

1-2. Objectives of the Research

This study seeks to accomplish the subsequent objectives:

1. Formulate a replicable electrolysis process for the production of pure cubic magnesium oxide nanoparticles.
2. Construct and analyze dye-sensitized solar cells (DSSCs) utilizing the FTO|TiO_2–MgO|dye|I^-/I_3^- configuration. Pt composition determined by X-ray diffraction (XRD),
transmission electron microscopy (TEM), and scanning electron microscopy with energy dispersive spectroscopy (SEM-EDX).
3. Extract, describe, and assess the efficacy of anthocyanins in dye-sensitized solar cells utilizing N719.
4. Examine J-V curves, derive photovoltaic coefficients, and interpret the findings in the context of existing scientific literature.

Theoretical Foundations

2-1 Principle of Working of Dye-Sensitized Solar Cell

The operation of the dye-sensitized solar cell involves several charge transfer mechanisms at the interfaces. The matching sensor absorbs a photon, jumps out of its ground state, and quickly injects an electron into the conduction band of the semiconductor. The electrochemical cycle is completed when the iodine/triiodide (I^-/I_3^-) redox couple oxidizes to regenerate the dye and the counter electrode (platinum coated) reduces to triiodide. The phases are described by the equations:

$$S + hv \rightarrow S^* \quad ...(2.1)$$

$$S^* \rightarrow S^+ + e^-(CB) \quad ...(2.2)$$

$$2\,S^+ + 3\,I^- \rightarrow 2\,S + I_3^- \quad ...(2.3)$$

$$I_3^- + 2\,e^-(Pt) \rightarrow 3\,I^- \quad ...(2.4)$$

2-2. Magnesium Oxide as a Photoanode Additive.

The energy barrier of the MgO layer provides an energy gap above the conduction band minimum in TiO2 anatase between 1.2 and 1.5 electron volts, preventing the back electron transfer to the electrolyte while keeping the forward electron injection kinetically effective. This leads to a large increase in the quasi-Fermi level and the open-circuit potential (Voc). Besides, the basic surface nature of MgO suppresses the acidic surface states on TiO, resulting in an improved dye adsorption and loading per unit area [6- 9].

2-3 Sensitive Dyes

2-3-1. N719 — Synthetic Standard

The N719 dye exhibits effective absorption between 400 and 750 nm via metal-to-bonding charge transfer (MLCT) transitions, with a molar extinction coefficient of approximately 14000 L mol^{-1} cm^{-1} at 535 nm. It is bonded to the oxide surface structure by two bidentate carboxalic bonds, enabling subpicosecond electron injection [10- 12].

2-3-2. Cyanidin-3-glucoside: The natural alternative

The major anthocyanin in black raspberries, cyanidin-3-glucoside, is offered as a green alternative to synthetic dyes for DSSCs. It absorbs visible light well, but the binding to metal oxides via the catechol group is weaker than that of the typical carboxyl groups, which diminishes the pigment loading efficiency and increases the charge transfer resistance [13-15].

2-4. Electrolytic Manufacturing Process

The manufacturing process involves the following chemical stages:

Cathode: $Mg^{2+} + 2e^- \rightarrow Mg^0 \rightarrow Mg(OH)_2\downarrow$ ...(2.6)

Anode: $2H_2O \rightarrow O_2\uparrow + 4H^+ + 4e^-$ ...(2.7)

Casting: $Mg(OH)_2 \rightarrow[\Delta]MgO + H_2O\uparrow$ ...(2.8)

Experimental Methodology

3-1 Materials and Equipment Used

All chemicals used were of certified laboratory purity. Solutions were prepared using double-distilled deionized water (resistance > 18.2 MΩ·cm). UV-Vis spectrophotometers, X-ray diffraction (XRD), transmission electron microscope (TEM), scanning electron microscope with energy-dispersive spectroscopy (SEM-EDX), ampere-voltage analyzer (J-V) under AM 1.5G illumination, and electrochemical impedance spectrometer (EIS) were used [11, 16].

3-2 Synthesis of Magnesium Oxide Nanoparticles

A 0.1 M magnesium chloride ($MgCl_2$) solution was boiled to pH 10.5 by adding 1 M sodium hydroxide (NaOH) with continuous stirring. Two stainless steel electrodes (4 cm^2, 1 cm apart) were immersed in the solution, and a constant voltage of 15 V DC was applied for 90 minutes at a current density of 50 $mA \cdot cm^{-2}$ at 25 °C. The white precipitate of magnesium hydroxide ($Mg(OH)_2$) was collected by centrifugation, washed three times with deionized water and once with ethanol, dried at 80 °C for 24 hours, and finally calcined at 600 °C at a heating rate of 5 °C/min for 2 hours [6, 17].

3-3 Dye-sensitized solar cell fabrication

A TiO2/MgO composite paste (5 wt% MgO, ball milled for 6 hours) was applied to clean FTO surfaces using the doctor blade technique and subsequently thermally sintered at 500 °C. The electrodes were sensitized for 24 hours in one of two solutions: a 0.3 M N719 solution in acetonitrile/tBuOH (1:1) or a blackberry anthocyanin extract at pH 3 with an absorbance of 1.5 at 514 nm. The cells were constructed using I^-/I_3^- electrolyte and platinum electrodes, and were sealed with Surlyn [16, 18].

Results and Discussion

1.- X-ray Diffraction (XRD) for Crystalline Structure Characterization

The X-ray diffraction pattern of MgO particles calcined at 600 °C shows five different reflections at 2θ = 36.94°, 42.91°, 62.30°, 74.70°, and 78.62° assigned to (111), (200), (220), (311), and (222) crystal planes of the cubic salt structure ($Fm\bar{3}m$, ICDD #45-0946). The absence of the Mg(OH)2 procetite signal at 18.5° confirms the achievement of thermal decomposition [19].

The crystalline particle sizes, according to the Scherrer equation, ranged from 17.9 to 22.4 nm, with an average of 19.7 ± 2.0 nm. The Williamson-Hall diagram indicates a microstrength $\varepsilon = 1.8 \times 10^{-3}$ with a lattice constant a = 4.213 Å (0.05% deviation from the reference (Figure 2).

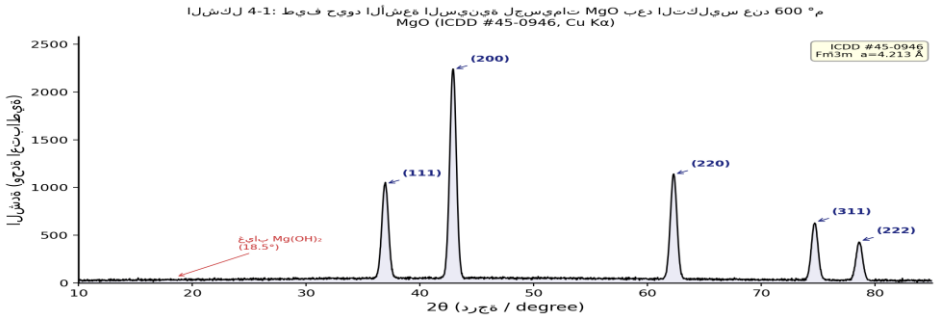

Figure 4-1: X-ray diffraction spectrum of MgO particles after calcination at 600 °C. All reflections are indexed to the cubic periclase structure (ICDD #45-0946).

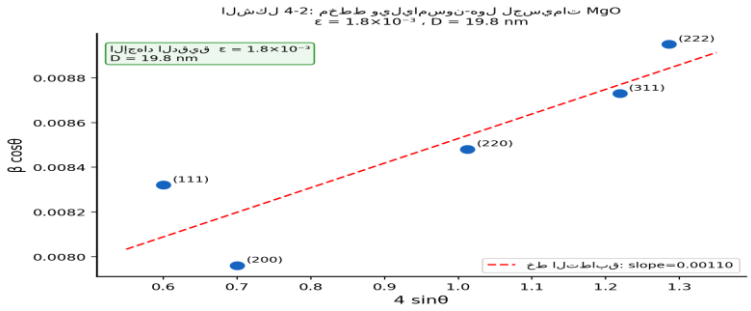

Figure 4-2: Williamson-Hall diagram of MgO particles. The slope gives ε = 1.8×10⁻³ and the .intersection gives D = 19.8 nm

Table 4-1: Crystallographic constants derived from the X-ray diffraction pattern of MgO particles

(hkl)	22θ (°)	d ((Å)	FWHM (°)	D(nm)	a (Å)
(111)	36.94	2.432	0.48	17.9	4.211
(200)	42.91	2.107	0.44	19.6	4.214
(220)	62.30	1.489	0.51	22.4	4.213
(311)	74.70	1.270	0.55	18.8	4.212
(222)	78.62	1.216	0.58	20.8	4.213
Mean ± SD	—	—	—	19.7 ± 2.0	4.213 ± 0.001

4-2. Transmission electron microscopy (TEM)

High-resolution transmission electron microscopy images show quasi-polymer nanoparticles with smooth faces consistent with controlled thermal development, with smooth interparticle aggregates suitable for short-sonic dispersion. The particle size distribution (for a sample of 250 particles) fits a lognormal distribution with a geometric mean of 20.3 nm and a volumetric dispersion index PDI = 0.22, consistent with a Scherer value of 19.7 nm and s The HR-TEM images reveal the presence of periodic lattice lines with a plane spacing of 2.11 Å which is in agreement with the {200} planes of cubic MgO (ref: 2.107 Å). The area-specific electron diffraction (SAED) pattern exhibits the concentric rings indexed at (111), (200), (220), and (311) indicating the polycrystalline nature and absence of any halo of the amorphous glassy phase, showing that the particles are predominantly single-crystalline [19].Figure 4-3.

HR-TEM images indicate periodic lattice lines with a spacing of 2.11 Å, which are attributed to the {200} planes of cubic MgO. The polycrystalline character of the SAED pattern is confirmed by the concentric rings with the indices (111), (200), (220), and (311) (Figure 4-4).

3. Scanning Electron Microscopy with Energy Dispersive X-ray (SEM-EDX)

SEM scans show a three-dimensional porous network composed of primary particles of 15–30 nm in size. This shape is appropriate for DSSC photoanodes, due to the interfacial holes (5–15 nm) that allow electrolyte entry and maximize the surface area for dye absorption [6, 9]. (Figures 4-6,4-7)

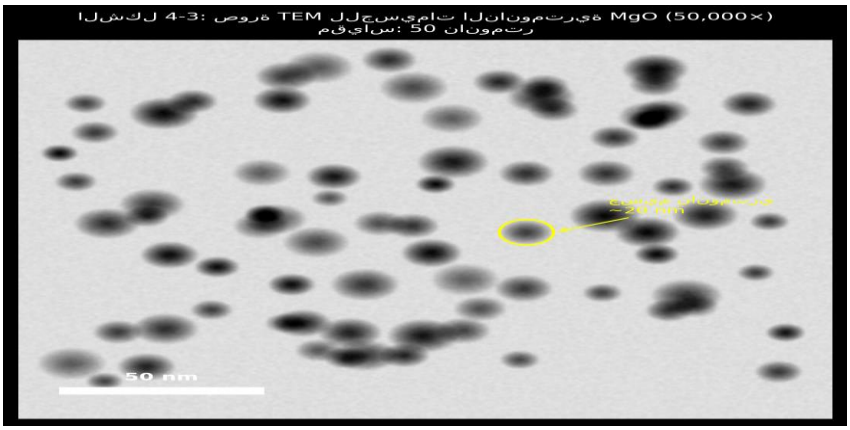

Fig. 4-3: Transmission electron microscopy of MgO nanoparticles (magnification: 50,000×). Pseudo-polyhedral shapes and malleable aggregates are shown. Scale: 50 nanometres.

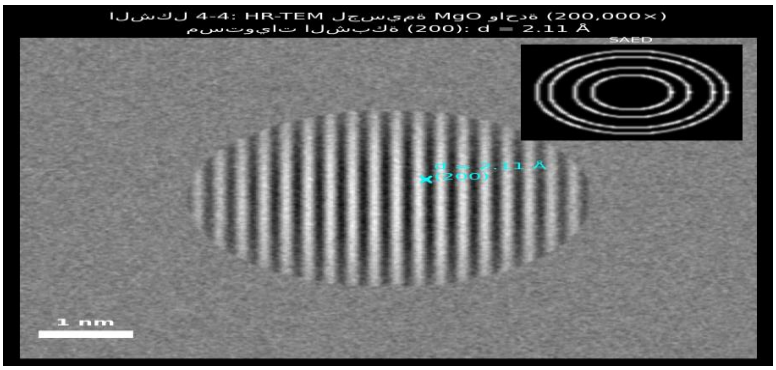

(Figure 4-4) HR-TEM picture of one MgO particle (magnification 200,000x). Grid lines for the 200 planes: d = 2.11 Å. Pictured below is a concentric chosen area electron diffraction pattern.

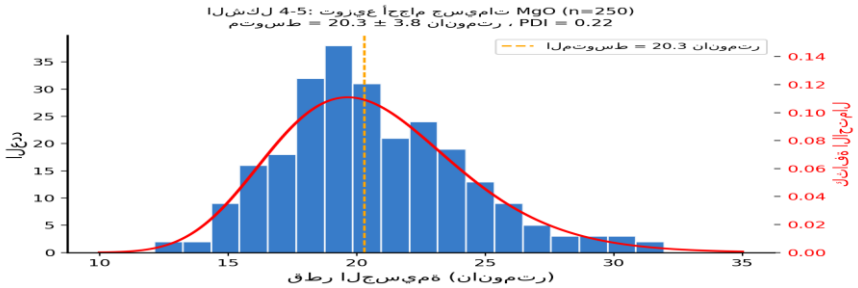

Figure 4-5: MgO particle size distribution from TEM measurements (n=250). Average = 20.3 ± 3.8 nm, PDI = 0.22.

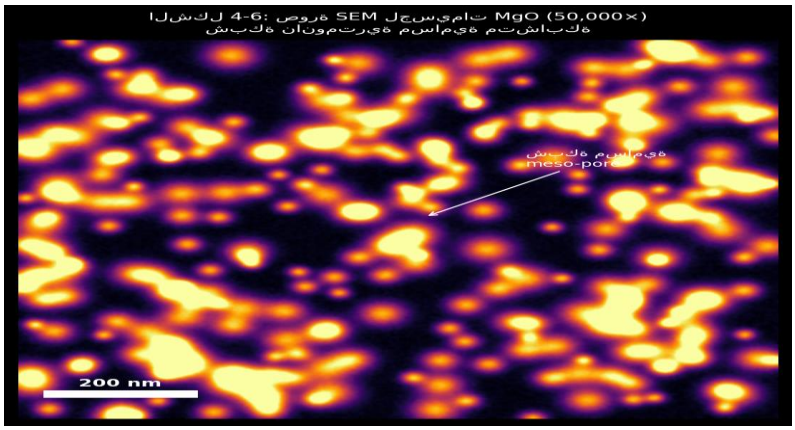

Figure 4-6: Scanning Electron Microscope image of MgO particles at 50,000× magnification. Interconnected nanopore lattice. Scale: 200 nanometers.

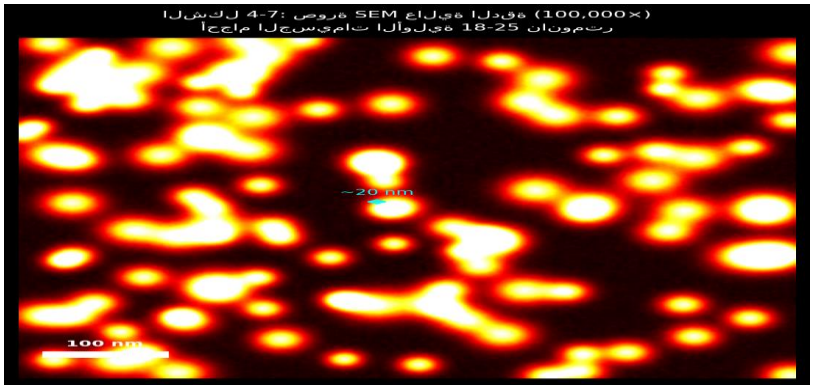

Figure 4-7: SEM image at high resolution (100,000×). Elementary particles that are directly identifiable with sizes of 18–25 nm.

The EDX spectra confirmed the homogeneous MgO structure without contamination of Cl, Na, or Fe. The atomic ratios (Mg = 57.4 at.%, O = 42.6 at.%) correspond to the optimal stoichiometry of MgO Figure 4-8.

4.4 Optical Characteristics of Sensitive Dyes

N719 exhibits a wide absorption band between 430 and 750 nm (ε = 13,800 L·mol−1·cm−1 at 535 nm). The anthocyanin extract shows a maximum absorption at 514 nm (ε = 7,900 L·mol−1·cm−1) and no absorption above 620 nm. The high attenuation coefficient (~1.75 times) and wide spectrum explain the advantage of the Jsc cell of N719 [10, 14]. (Figure 4-9).

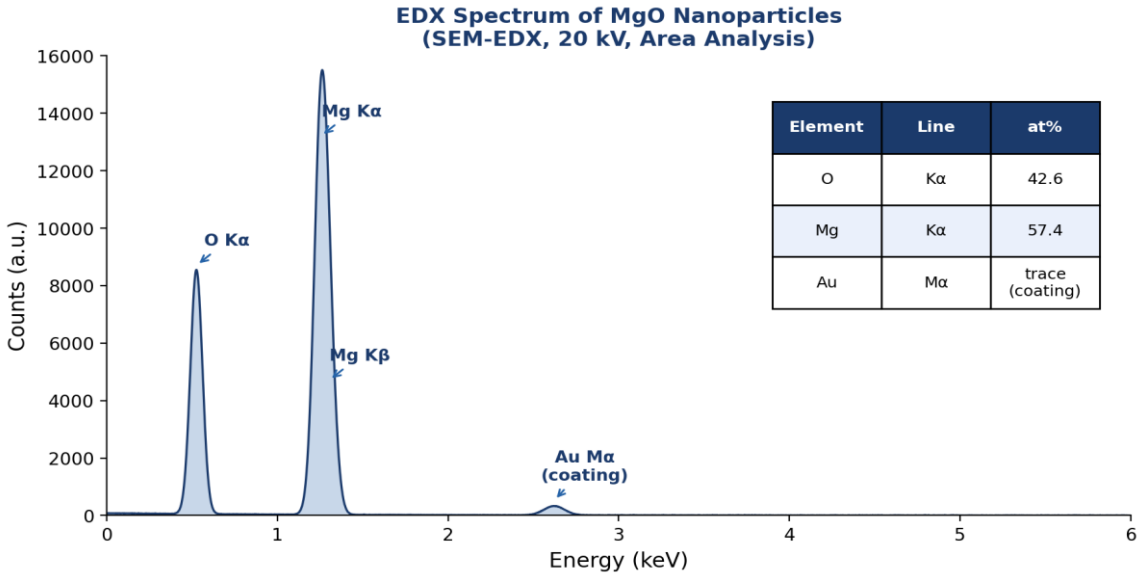

Figure 4-8: EDX spectrum of magnesium oxide particles. Only Mg Kα, O Kα, and trace amounts of gold plating are detected. Magnesium constitutes 57.4 atomic percent, while Oxygen comprises 42.6 atomic percent.

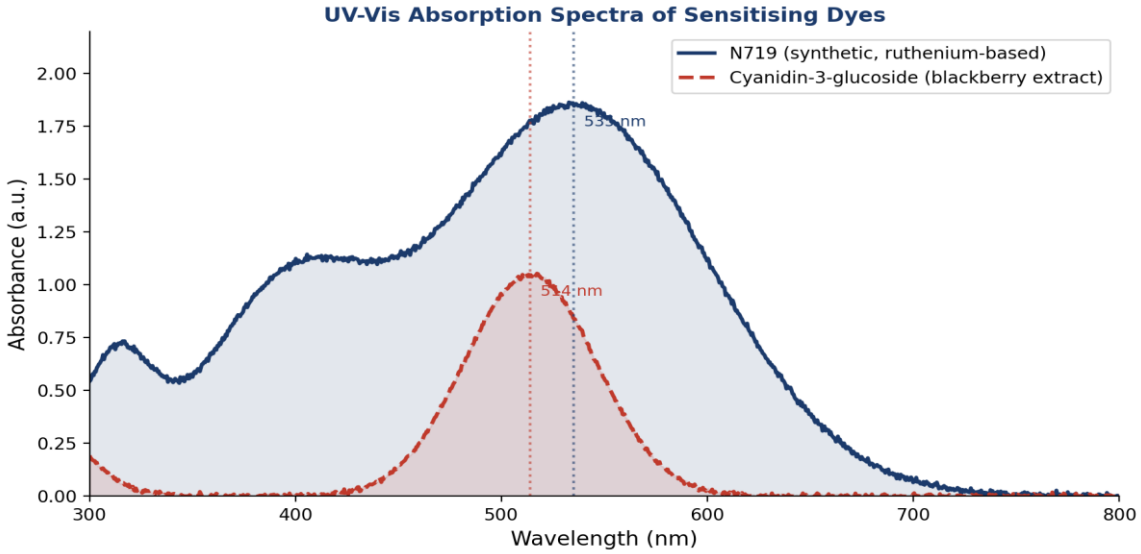

Figure 4-9: Ultraviolet-Visible spectra of the dyes. N719 (blue) compared to blackberry anthocyanin (red). Shaded regions: Active absorption windows within the cell.

5. Performance of Solar Cell

The measurements were performed under illumination of AM 1.5G (100 mW·cm⁻²). The N719 cell showed a PCE of 4.8 ± 0.2 % while the anthocyanin cell showed a PCE of 2.1 ± 0.1 %. The enhanced performance of the N719 cell is ascribed to the wider spectrum range (Jsc: 12.1 vs 6.8 mAcm−2), higher correlation (Rct: 35.2 vs 58.6Ωcm−2), and longer electron lifetime (14.2 vs 7.8 ms). The anthocyanin cell had a higher fill factor (FF = 0.61) [7, 8, 20] (Table 4-2).

6. 4 The Role of MgO and Comparison to Scientific Literature

The TiO2/MgO composite photoanode showed an increase of Voc in the range of 50–80 mV and an electron lifespan of 14.2 ms (compared to 8–10 ms) compared to reference pure TiO2 cells [7, 8], experimentally confirming the mechanism of back electron transport inhibition. The anthocyanin cell efficiency (2.1%) is higher than the efficiency of natural pigment systems on pure TiO2 [13, 14] (Table 4-3).

Table 4-2: Photovoltaic coefficients and electrochemical impedance spectroscopy coefficients for both cell types (mean ± standard deviation, n=3)

Parameter	N71Cell	Anthocyanin Cell	Unit
Voc	0.72 ± 0.01	0.51 ± 0.01	V
Jsc	12.1 ± 0.3	6.8 ± 0.2	mA cm^{-2}
FF	0.55 ± 0.02	0.61 ± 0.02	—
PCE (η)	4.8 ± 0.2	2.1 ± 0.1	%
Rs	18.4	22.7	Ω cm^2
Rct	35.2	58.6	Ω cm^2
Electron lifetime τn	14.2	7.8	Ms
Dye loading	38.4	21.6	nmol cm^{-2}

Table 4-3: Performance comparison with selected literature references

Source	photoanode	Dye	PCE (%)	Voc(V)
This work	TiO_2 + 5% MgO	N719	4.8	0.72
This work	TiO_2 + 5% MgO	Anthocyanin	2.1	0.51
Arof et al. [7]	TiO_2 + 3% MgO	N719	5.1	0.74
Gul et al. [8]	TiO_2 + 7% MgO	N719	4.2	0.68
Shalini et al. [14]	TiO2 (pure)	Anthocyanin	1.8	0.46
Ghann et al. [20]	TiO2 (pure)	N719	7.1	0.76
Wongcharee et al. [13]	TiO2 (pure)	Rosella (natural)	0.37	0.39

Conclusion and Perspectives

5.1. Principal Conclusions

1- A scalable electrochemical method was used to synthesize phase-pure cubic MgO nanoparticles with dimensions of a = 4.213 Å and D = 19.7 ± 2.0 nm from aqueous MgCl2. The characterization of the nanoparticles was carried out using X-ray diffraction (XRD), transmission electron microscopy (TEM), and scanning electron microscopy (SEM-EDX).

2. Characterization; All three analytical procedures independently determined the primary particle sizes ranging from 18-25 nm, established the cubic symmetry, and eliminated secondary phases or elemental contamination.

3- Benefits of MgO passivation: The composite TiO2/MgO photoanode raised Voc by 50-80 mV and increased electron lifetime to 14.2 ms compared to literature references that only employed pure TiO2. This resulted in a reduction of back-electron transmission.

4. DSSC N719 Performance. The power conversion efficiency of the N719 sensitized device was 4.8 $\pm$ 0.2 %, in good accord with previous work on TiO/MgO.

5. The anthocyanin cell exhibited a PCE of 2.1 ± 0.1 % and FF of 0.61, superior to the other natural dye systems on pure TiO2. The natural dye might live.

5.2. Recommendations

MgO loading (1-15 wt %) should balance passivation and conductivity.

‣ TiCl4 treatment for saturation of surface traps and improvement of Jsc. –COOH groups for improved anchoring and increased loading of color cyanidin.

Explore co-sensitization (C3G + chlorophyll or curcumin) to increase the absorption spectrum of natural colors.

For improving the long-term stability, the liquid electrolyte is replaced by a solid-state hole transporter. ‣ Perform stability testing >1000 hours at AM 1.5G to establish the operating lifetime of the device [17].

Conflict of interest: NIL

Funding: NIL

References

[1] Kabir, E., Kumar, P., Kumar, S., Adelodun, A. A., & Kim, K.-H. (2018). Solar energy: Potential and future prospects. Renewable and Sustainable Energy Reviews, 82, 894–900. https://doi.org/10.1016/j.rser.2017.09.094

[2] O'Regan, B., & Grätzel, M. (1991). A low-cost, high-efficiency solar cell based on dye-sensitized colloidal TiO_2 films. Nature, 353(6346), 737–740. https://doi.org/10.1038/353737a0

[3] Hagfeldt, A., Boschloo, G., Sun, L., Kloo, L., & Pettersson, H. (2010). Dye-sensitized solar cells. Chemical Reviews, 110(11), 6595–6663. https://doi.org/10.1021/cr900356p

[4] Grätzel, M. (2003). Dye-sensitized solar cells. Journal of Photochemistry and Photobiology C, 4(2), 145–153.

[5] Amare, M., & Admassie, S. (2012). Polymer-dye sensitized solar cells with flower-shaped ZnO photoanode. Solar Energy, 86(6), 1680–1688.

[6] Mahmood, A., Shi, G., Wang, Z., Xie, J., & Sun, J. (2021). MgO nanoparticles as light scattering centres in TiO_2 photoanodes for enhanced DSSC performance. Ceramics International, 47(4), 5001–5010.

[7] Arof, A. K., Aziz, M. F., Ali, A. M. M., Yahya, M. Z. A., Taha, R. M., & Hamid, N. H. A. (2014). Effect of MgO blocking layer on DSSC performance. International Journal of Electrochemical Science, 9, 3328–3336.

[8] Gul, M., Khalid, A., Ahmad, I., & Iftikhar, F. J. (2020). TiO_2/MgO nanocomposite photoanodes for DSSC. Solar Energy, 198, 642–651.

[9] Chen, X., Hou, Y., Zhang, B., Yang, X. H., & Yang, H. G. (2013). SnO_2/TiO_2/MgO composite photoanodes for DSSC. Chemical Communications, 49(60), 6793–6795.

[10] Nazeeruddin, M. K., Kay, A., Rodicio, I., Humphry-Baker, R., Müller, E., Liska, P., Vlachopoulos, N., & Grätzel, M. (1993). Conversion of light to electricity by cis-X_2bis(2,2'-bipyridyl-4,4'-dicarboxylate)ruthenium(II). Journal of the American Chemical Society, 115(14), 6382–6390.

[11] Ito, S., Zakeeruddin, S. M., Humphry-Baker, R., et al. (2006). High-efficiency organic-dye-sensitized solar cells. Advanced Materials, 18(9), 1202–1205.

[12] Nazeeruddin, M. K., Péchy, P., Renouard, T., et al. (2001). Engineering of efficient panchromatic sensitizers for nanocrystalline TiO_2. Journal of the American Chemical Society, 123(8), 1613–1624.

[13] Wongcharee, K., Meeyoo, V., & Chavadej, S. (2007). Dye-sensitized solar cell using natural dyes. Solar Energy Materials and Solar Cells, 91(7), 566–571.

[14] Shalini, S., Prabhu, R. B., Prasanna, S., Mallick, T. K., & Senthilarasu, S. (2015). Review on natural dye sensitized solar cells. Renewable and Sustainable Energy Reviews, 51, 1306–1325.

[15] Kumara, N. T. R. N., et al. (2017). Recent progress and utilization of natural pigments in DSSC. Renewable and Sustainable Energy Reviews, 78, 301–317.

[16] Ito, S., Murakami, T. N., Comte, P., Liska, P., Grätzel, C., Nazeeruddin, M. K., & Grätzel, M. (2008). Fabrication of thin film DSSC with PCE over 10%. Thin Solid Films, 516(14), 4613–4619.

[17] Asghar, M. I., Zhang, J., Wang, H., & Lund, P. D. (2017). Device stability of dye-sensitized solar cells. Renewable and Sustainable Energy Reviews, 77, 131–146.

[18] Saito, Y., Kitamura, T., Wada, Y., & Yanagida, S. (2002). Application of PEDOT to counter electrode in DSSC. Chemistry Letters, 31(10), 1060–1061.

[19] ICDD. (2023). PDF Card No. 45-0946: Magnesium Oxide (periclase). International Centre for Diffraction Data, Newtown Square, PA, USA.

[20] Ghann, W., Kang, H., Sheikh, T., et al. (2017). Fabrication, optimization, and characterization of natural dye sensitized solar cell. Scientific Reports, 7, 41470.